Spacecraft Momentum Unloading: The Cell Mapping Approach

H. Flashner*
University of Southern California, Los Angeles, California
and
T. F. Burns†
TRW, Inc., Redondo Beach, California

An approach for developing spacecraft angular momentum unloading control algorithms based on the cell mapping formulation is presented. Representations of periodic dynamic systems in terms of point mappings are discussed and their discretizations to form cell mappings derived. An optimal control technique exploiting the cell approach is presented and applied to the problem of momentum unloading. A number of unloading schemes by means of magnetic torquers are derived using this cell state space optimal control approach. The unloading schemes entail off-line control sequence generation, enabling the attitude control system to achieve unloading by a table lookup of magnetic torquer settings once per orbit. Simulation study results for two model spacecraft in low Earth orbit indicate closely bounded momentum performance from the control laws developed by the proposed approach.

Nomenclature

A_y, A_z = constant coefficients in disturbance model equations
$\boldsymbol{B}$ = magnetic field
$b_i(t)$ = magnetic field component, $i = 1,2,3$
C = cell mapping; number of control levels
$f(\,.\,,\,.\,)$ = vector function
$G_{i/k}$ = short for $\int_{[n+(i-1)/k]T}^{(n+i/k)T} \boldsymbol{B}(\tau)\,d\tau$
g = point mapping
$\boldsymbol{H}$ = angular momentum
H_i = component of angular momentum
$H_{\max}$ = control moment gyro maximum angular momentum value
h_{cx}, h_{cy}, h_{cz} = control moment gyro angular momenta
h_i = cell length in ith dimension
I_x, I_y, I_z = principal moments of inertia
J = cost function
K_{px}, K_{py}, K_{pz} = proportion feedback gains, attitude control law
K_{rx}, K_{ry}, K_{rz} = rate feedback gains, attitude control law
$\boldsymbol{M}$ = magnetic moment
$M_{\max}$ = maximum magnetic moment value
N = number of cells in cell state space
P = number of possible control sequences
q = dimension of state space
S_y, S_z = constant coefficients in disturbance model equations
$\boldsymbol{T}$ = torque
T = orbital period; number of table entries in control/state-space table
T_{abx} = disturbance torque, body frame, x component
T_{aby} = disturbance torque, body frame, y component
T_{abz} = disturbance torque, body frame, z component
T_{cx}, T_{cy}, T_{cz} = attitude control torque, dynamics equations
T_{dx}, T_{dy}, T_{dz} = disturbance torque, dynamics equations
t = time
u = control vector
V = discrete control vector
W_1, W_2 = cost function weighting matrices
w = momentum threshold to apply alternate unloading sequence set
x = q-dimensional state
z = cell state variable
θ = attitude pitch angle
τ = time
ϕ = attitude roll angle
ψ = attitude yaw angle
ω_0 = spacecraft angular rate

Received Dec. 22, 1987; revision received June 3, 1988.

*Assistant Professor, Department of Mechanical Engineering. Member AIAA.
†Member, Technical Staff, Space and Defense Sector. Member AIAA.

I. Introduction

THE problem of momentum management has always been a significant issue in control system design for spacecraft. Large size and longer lifetime requirements of modern spacecraft have caused this issue to become one of the most critical requirements of future space missions. Typical modern spacecraft momentum management requirements as formulated for the space station are given by Woo et al.[1]

Most momentum management schemes employ the interaction of the spacecraft with the environment to generate the needed unloading torques. Gravity gradient torques were used by Shain and Spector[2] to develop a torque equilibrium attitude control scheme that also incorporates momentum unloading. This approach was developed further by Woo et al.[1] by applying optimal control theory to the derivation of the control law. An alternative approach to momentum unloading is to employ Earth's magnetic field. Magnetic attitude control has been discussed extensively in the literature and has been implemented in practice.[3,4] Magnetic torquing for momentum unloading using the cross product and minimum energy control laws is discussed in reports by NASA[5] and BellCom.[6] Applications of these magnetic unloading control laws to specific spacecraft configurations are discussed by Junkins et al.[7] and Decanini et al.[8]

Existing magnetic momentum unloading control laws have a number of shortcomings. The cross-product control law produces unloading torques based on the instantaneous value of the accumulated momentum. The goal, however, of an unloading law is to prevent momentum buildup by dumping the secular component of the accumulated momentum. Therefore, a torque proportional to the total momentum may require unnecessarily high magnetic moments. Moreover, since

the cross-product control law operates on instantaneous information, it ignores the fact that for a given orbit the orientation of the spacecraft with respect to the direction of the magnetic field can be predicted. By using this knowledge, one can apply unloading torque about the various axes at locations when the direction of the magnetic field is favorable. The minimum energy unloading control law is an open-loop control scheme that assumes complete knowledge of the magnetic field during the entire orbit. The secular component of the momentum is unloaded over one orbit using a predetermined optimal scheme that requires extensive real-time calculations. The resulting control law is very sensitive with respect to perturbations in the magnetic field model and, as with all open-loop schemes, cannot counteract unexpected disturbance torques.

This study presents a new approach to the development of momentum unloading control laws that overcomes many of the shortcomings of the previously mentioned techniques. This new approach is based on the cell mapping analysis concept introduced by Hsu[9-13] and subsequently extended to control systems.[14] The cell mapping control approach is a scheme that assumes predetermined discrete control levels over fixed time intervals. It allows maximum utilization of favorable environmental magnetic field conditions, as does the minimum energy law, but is particularly advantageous in that all of the computations are performed off-line. The optimal magnetic settings are accessed via a table-read, which is extremely simple to implement and results in a near-autonomous unloading ability. In addition, the optimality of the method is keyed directly to the available discrete control levels of the electromagnetic actuators. The cell mapping approach is well-suited for the momentum unloading problem in particular, because momentum wheel or control moment gyro (CMG) momentum behaves as an almost periodic system. It will be demonstrated that expressing a dynamic system in periodic form is the key to the applicability of cell mapping to control.

This paper is organized as follows: Section II presents a general discussion of cell mapping and cell state-space optimal control (CSSOC). Section III discusses the attitude control model and environmental models used for validation of the new momentum unloading concept. Section IV details the application of CSSOC to momentum unloading. Section V presents the simulation results using the new technique.

II. Cell Mapping and Cell State Space Optimal Control

Following closely the work of Hsu,[9-13] we introduce the cell mapping approach to the analysis of dynamic systems. We present the application of cell mapping to the analysis of control systems as formulated by Hsu[14] and extend it to time-varying systems. This extension allows the application of the cell mapping approach to the design of a momentum unloading control algorithm.

A. Cell Mapping Representation of Dynamic Systems

For realistic dynamic systems, the performance of a closed-loop control law can be specified to be within finite bounds. This is because of the finite accuracy of both the actuators and sensors due to the effects such as friction, hysteresis, dead zone, etc. However, modern control laws are implemented on digital computers whose accuracy is limited by quantization due to roundoff and truncation errors, and by finite wordlength. Therefore, in modeling dynamic systems, there exists a threshold beyond which increased refinement of modeling no longer enhances control system performance. The cell mapping concept is an approach to discretizing the state space into cells of size consistent with control design requirements. The main advantage of the approach is that it is especially suitable for analysis on modern computers and, therefore, can be applied to realistic systems (possibly nonlinear and time varying).

Given a dynamic system in state-space form as

$$\dot{x}(t) = f(x,t) \tag{1}$$

where x is a q-dimensional state vector and f a q-dimensional vector field, in general nonlinear. If f is a periodic function of time, then the dynamics of the system in Eq. (1) are defined by a mapping that relates the state of the system in the beginning of the period to the state at the end of the period. This mapping, called a point mapping or Poincare map, can be expressed in the form of difference equations:

$$x(n+1) = g[x(n)] \tag{2}$$

where $g(\ )$ is a q-dimensional function, $x(n)$ the state vector at the beginning of the period, and $x(n+1)$ the state at the end of the period. By employing the notion of point mapping, the system of time-varying, nonlinear differential equations of Eq. (1) has been transformed in Eq. (2) into a set of nonlinear difference equations that no longer depends on time. A trajectory of Eq. (2) starting at the initial state $x_0(0)$ is the sequence $\{x_0(k)\}$, $k = 0,1,2,\ldots$. The point mapping $g(\ )$ can be determined analytically for certain specific types of systems or by numerically integrating the system [Eq. (1)] over one period of time.

The cell mapping representation of a dynamic system is obtained by first discretizing the state of the system. The discretization is achieved by dividing the state space into regions identified by the cell state variable Z, where Z takes on only integer values according to the following rule:

$$(Z_i - \tfrac{1}{2})h_i < x_i < (Z_i + \tfrac{1}{2})h_i, \qquad i = 1,2,\ldots,q$$

Here h_i is the cell size in the direction of the Z_i axis.

The cell mapping is then expressed as a discrete mapping

$$Z(n+1) = C[Z(n)] \tag{3}$$

$Z(n)$ and $Z(n+1)$ represent the discrete cell *domain* and *image*, respectively, of the cell state variable Z. C is a cell mapping obtained either from the point mapping g of the periodic system or by integrating the system [Eq. (1)] over one period of time. A cell state-space trajectory of Eq. (3) starting at the initial cell state $Z_0(0)$ is represented by the set of integers in the cell sequence $\{Z_0(k)\}$, $k = 0,1,2,\ldots$. The dynamic behavior of cells, including those exhibiting limit cycles, and their domains of attraction can be determined by using an unraveling algorithm of global analysis as outlined by Hsu[10] and Guttalu.[11]

Unlike analysis in the continuous state space, analysis in the cell state space covers a finite breadth of q space. The state space of interest to the observer is fully discretized into cells, and the remainder of the state space extending to infinity is lumped into one additional cell called the *sink cell*. If the trajectory moves into the sink cell, it is automatically regarded as being of no further interest. Each point of the state space fits into one of the defined cells, or the sink cell. Each defined cell is represented by one point in the cell, typically, but not restricted to, the center point of that cell. Every state-space position within the boundaries of that cell is regarded as having the value of the cell.

B. Control System Analysis Using Cell Mapping

Consider a periodic system with a period τ, which is controlled by the vector $u(t)$. Assume that the control level can change only in the beginning of the period. This assumption is equivalent to saying that the system is controlled by a discrete-time controller with sampling time τ starting at $t = 0$ and that a zero-order hold is implemented. In terms of a point mapping, the equations of the controlled system are the following:

$$x(n+1) = g[x(n),u(n)] \tag{4}$$

Now consider the scenario whereby the control $u(n)$ can be applied only at a finite number of discrete levels. Let this discrete control be given by vector V. In control terminology, it means that the controller possesses a finite number of quantization levels. Then the dynamics of the system can be expressed by cell mapping:

$$Z(n+1) = C[Z(n), V(n)] \tag{5}$$

The cell mapping representation given in Eq. (5) expresses the dynamics of the system in terms of finite, discrete values of the state and control vectors. We shall assume that the objective of the control effort is to bring the system to a predetermined region of the state space (a *target set* in terms of cell state space) while minimizing a performance index J (cost). The cell mapping formulation facilitates the development of efficient numerical algorithms for computation of an optimal sequence $V(n)$. Hsu[14] has developed a technique for control design called cell state space optimal control (CSSOC) that involves the determination of the optimal control of a dynamic system by a numerical search process. A table called control/state space table (CSST) is created. This table possesses the image cells $Z(n+1)$ of every cell $Z(n)$ under all possible control levels $V(n)$. The CSST is processed into a cell state space optimal control table (CSSOCT) by a dynamic programming-type procedure as follows:

1) A first pass through the CSST searches for the control level that maps a given domain cell to the target set in one mapping step, at lowest cost.

2) Cells that converge to the target set in one step are added to the target set, creating an augmented target set of cells that converge to the target set in one step or less. These cells and their associated lowest-cost controls are saved in the CSSOCT and are purged from the CSST.

3) A second pass through the CSST searches for the lowest-cost control to bring each cell in the now-reduced set of domain cells to the augmented target set. Domain cells that converge are added to the target set, creating a new target set of cells that reach the original target set in two steps or less. The converging domain cells and their associated lowest-cost controls are again added to the CSSOCT.

4) This process continues until either the entire cell state space is assigned the lowest-cost control or until all of the controllable state cells are assigned their lowest-cost control. Some cells may be found to be uncontrollable in the sense that none of the acceptable controls in any number of passes will drive a domain cell to an image cell that, by using successive steps, finds its way to the original target set.

When the creation of the CSSOCT is complete, it contains the optimal control for each controllable domain state. That is, the control value that results in the trajectory attaining the original target set at the lowest cost in the minimum number of mapping steps.

III. Simulation Models

Coordinate systems referred to in this paper are the body coordinate frame and the reference coordinate frame. They are defined in Appendix A.

A functional block diagram of the attitude control system simulated in this study is shown in Fig. 1. Note that the system possesses two interacting control loops: one for attitude control and one for momentum unloading. The control system can be designed in two stages: first, the attitude control loop is closed to achieve the required transient response; then the momentum unloading loop is designed considering the spacecraft with the closed attitude loop as the plant. By using this approach, control torques of each loop are considered to be disturbances acting on the other loop. The separate design of the two loops is often used (see, for example, Junkins et al.[7]) since the two subsystems, attitude control and momentum unloading, have bandwidths that differ by at least an order of magnitude. In the scheme used in this study, momentum

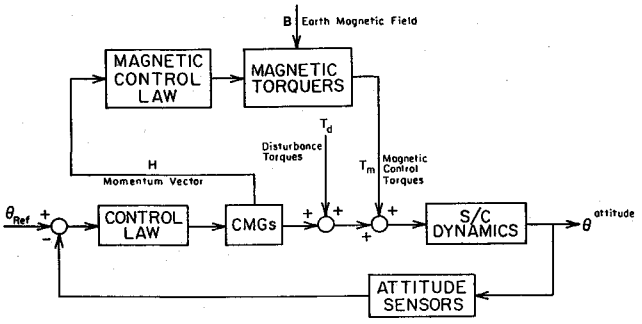

Fig. 1 Attitude and momentum unloading control systems.

unloading control changes at most every quarter-orbit, i.e., about every 1400 s for low Earth orbits, whereas the attitude control system has a time constant on the order of seconds.

The attitude controller employed for validation of the new unloading technique is of the proportional/rate type. We assume an Earth-pointing desired attitude. The attitude dynamics and attitude control equations are given in Appendix B.

The Earth's magnetic field is modeled in simulation to validate the new unloading technique by a tilted dipole representation derived by Wheeler.[15] The choice of a simple model is based on the determination that simple magnetic field models have served in the past as design tools for quite adequate magnetic unloading algorithms.[16,17] The components of the tilted dipole model are given in Appendix C.

A simple model is chosen also to represent the nongravity gradient external disturbance torques, which are dominated by aerodynamic drag in a low Earth orbit. The following sinusoidal functions are employed (body coordinates):

$$T_{abx} = 0 \tag{6a}$$

$$T_{aby} = A_y \sin\omega_0 t + S_y \tag{6b}$$

$$T_{abz} = A_z \sin\omega_0 t + S_z \tag{6c}$$

where ω_0 is the orbit rate, and A_y, A_z, S_y, S_z are constant coefficients whose values are determined by estimating aerodynamic drag characteristics from previously established models depending on the orbit being simulated.[8,18] The x component is 0 due to the Earth-pointing attitude assumption. Junkins et al.[7] used a similar disturbance model.

IV. Momentum Unloading Cell State Space Optimal Control Law

The CSSOC method lends itself to applications of a periodic and discrete nature, possessing advantages over other methods of momentum unloading for the following reasons.

1) The stored angular momentum of a spacecraft has a dominant periodic component with the orbital period of the spacecraft. Furthermore, momentum unloading is a problem that must be dealt with on a long-term basis of many orbits, with concern focused on unloading the secular rather than the periodic component. The CSSOC method was developed from a periodic dynamic systems approach. Its implementation requires that the system be expressed in a periodic form.

2) Momentum control actuators include such devices as gas jets and magnetic torquers. These items generally produce control torque levels that are discrete and are best modeled as such. The CSSOC method produces optimal control sequences whose optimality is keyed to the specific discrete pattern of the control actuators' output.

A. Formulation of the Unloading Law in Terms of Cell Mapping

The cell state space optimal control table is created off-line using the cell mapping equations developed in this section and mated to the attitude control system for sampling every orbit.

In order to apply the cell mapping concept, the momentum unloading equations of the spacecraft need to be expressed in the form of a point mapping. To express the momentum/torque relationship in state-space form, note that, in general, in an inertial coordinate frame,

$$\boldsymbol{T} = \dot{\boldsymbol{H}} \tag{7}$$

Now consider $\dot{\boldsymbol{H}}$ to be the momentum wheel or CMG angular momentum rate of change due to magnetic control. The magnetic unloading torque is given by $\boldsymbol{T}_c = \boldsymbol{M} \times \boldsymbol{B}$. Thus, in state-space form,

$$\dot{\boldsymbol{H}} = -\boldsymbol{B}(t)\,\boldsymbol{M} \tag{8}$$

where

$$\boldsymbol{B}(t) = \begin{bmatrix} 0 & -b_3(t) & b_2(t) \\ b_3(t) & 0 & -b_1(t) \\ -b_2(t) & b_1(t) & 0 \end{bmatrix}$$

$b_i(t)$ are the components of the magnetic field vector as described in Appendix C, and $\boldsymbol{M}$ is the magnetic moment control. The state transition equation of the system [Eq. (8)] from time nT to $(n+1)T$ is then

$$\boldsymbol{H}[(n+1)T] = \boldsymbol{H}(nT) + \int_{nT}^{(n+1)T} -\boldsymbol{B}(\tau)\boldsymbol{M}(\tau)\,\mathrm{d}\tau \tag{9}$$

If T is the spacecraft orbital period, then we have achieved a point mapping representation of the system [Eq. (8)], where one mapping step is equivalent to one orbit.

Let the magnetic moment control $\boldsymbol{M}$ be a piecewise constant function. Let (T/k) be the length of the interval during which the control is constant, where k is an integer. Then Eq. (9) can be rewritten as

$$\boldsymbol{H}[(n+1)T] = \boldsymbol{H}(nT) - \sum_{i=1}^{k} \int_{[n+(i-1)/k]T}^{(n+i/k)T} \boldsymbol{B}(\tau)\,\mathrm{d}\tau\,\boldsymbol{M}_{i/k} \tag{10}$$

Equation (10) can be written symbolically as

$$\boldsymbol{H}[(n+1)T] = \boldsymbol{H}(nT) - \sum_{i=1}^{k} \boldsymbol{G}_{i/k}\boldsymbol{M}_{i/k} \tag{11}$$

It is desirable for the implementation of the CSSOC method to express Eq. (11) strictly as a function of the orbital period T. Equation (10) indicates that an expression for the magnetic field $\boldsymbol{B}(t)$, which is periodic in T, will enable this. The straight dipole model of the magnetic field is periodic in T. The straight dipole model assumes alignment of the Earth's dipole with its spin axis. It was found in this study and described earlier[15] that, for analyses such as this, considering one or more complete orbits, effects of dipole tilt nearly average to zero. Thus, for the creation of the CSSOCT from Eq. (11) the straight dipole model is chosen. See Appendix C for the straight dipole model equations.

The choice of the straight dipole model results in the sequence $G_{i/k}$, $i = 1,\ldots,k$ of Eq. (11) repeating itself every period T. If we assume that a control sequence over one orbital period is determined in the beginning of the period, then we can define $u(nT) = \{\boldsymbol{M}(nT),\ \boldsymbol{M}[nT+1/k),\ldots,\ \boldsymbol{M}[nT+(k-1)/k]\}$, and Eq. (11) takes the form of Eq. (4). Assuming discrete levels of the magnetic torque $\boldsymbol{M}$, the problem is then of the form of the cell mapping of Eq. (5). Thus, the momentum, $\boldsymbol{H}$, of Eq. (11) constitutes the three-dimensional state space, and $\boldsymbol{H}(n)$ and $\boldsymbol{H}(n+1)$ signify the domain and range, respectively, of the state $\boldsymbol{H}$.

The CSST described in Sec. II.B is created via off-line software by assuming a certain set of possible controls $\boldsymbol{M}$, which is finite and possesses discrete levels, and by computing Eq. (11) for every possible combination within that set. The CSSOCT is then generated (again off-line) following the algorithm of Sec. II.B. The CSSOCT in final form is a table containing discrete levels of CMG momentum $\boldsymbol{H}$ (domain states) vs k-numbered sequences of discrete levels of $\boldsymbol{M}$ (optimal control values).

Second-order effects, such as extra terms of the Earth's magnetic field model, as well as attitude control torques, environmental disturbance torques, and slowly varying orbital parameters, were modeled as disturbance torques acting on the unloading control of Eq. (11). It should be reiterated here that, for the CSSOCT generation, we assumed the straight dipole magnetic field model, but for validation of the new method through simulation we employed the more accurate model of the tilted dipole.

B. Computational Considerations

The storage requirements for implementing the CSSOC method vary considerably depending on the particular problem. If all of the cells in the discrete cell state space are found to have a control that causes convergence to the target set in one mapping step, then the CSST need not be stored at all. A CSSOCT can be generated directly. Otherwise, the CSST must be stored for multipass processing to generate the CSSOCT.

The size of the CSST, for a momentum unloading application, is a function of the number of discrete control levels and the per-orbit frequency with which the control is allowed to change. For example, if each orbit is divided into four segments of constant control, and there are two control levels, there will be $2^4 = 16$ possible control sequences. Similarly, for n levels, there will be n^4 possible control sequences. For a three-dimensional control vector and a discrete state space containing N cells, the number of table entries T to store in the CSST is $T = (P^3)N$, where P is the number of possible control sequences. If all of the data in a table entry is packed into one 8-byte record, the storage requirement for the CSST is $MB = 8(P^3)N/1 \times 10^6$, where MB is the number of megabytes of storage. Note that one may still utilize five- or seven-level control with reduced storage requirements by choosing a subset of the complete list of possible control sequences, thereby reducing P, and thus MB.

The CPU time requirements of the CSSOC method vary widely depending on whether the discrete control is segmented for each period, as in the preceding example, how many levels of discrete control one uses, and how complicated the cost function is.

C. Cost Function

The cost function is the function that the control is designed to minimize. Typically, it may be defined as

$$J = \int_0^T [\boldsymbol{H}'\boldsymbol{W}_1\boldsymbol{H} + \boldsymbol{M}'\boldsymbol{W}_2\boldsymbol{M}]\,\mathrm{d}t \tag{12}$$

where the prime indicates transpose, $\boldsymbol{W}_1$ and $\boldsymbol{W}_2$ are symmetric positive definite weighting matrices, and T is the orbital period. Thus, the momentum magnitude (i.e., the magnitude of the state) and the magnetic moment control magnitude are to be minimized according to the relative magnitudes of $\boldsymbol{W}_1$ and $\boldsymbol{W}_2$.

The integral of Eq. (12) is evaluated by using k-times-per-orbit sampling of $\boldsymbol{H}$ and $\boldsymbol{M}$. Also, since zero-order hold is implemented, $\boldsymbol{M}$ is constant over each T/k orbit segment. Integration of the terms containing $\boldsymbol{H}$ is performed using a trapezoidal approximation. Thus, Eq. (12) becomes

$$J = (T/k)\Bigg[(1/2)\boldsymbol{H}'_{\mathrm{dom}}\boldsymbol{W}_1\boldsymbol{H}_{\mathrm{dom}} + \sum_{i=1}^{k-1}\boldsymbol{H}'_{i/k}\boldsymbol{W}_1\boldsymbol{H}_{i/k} + (1/2)\boldsymbol{H}'_{\mathrm{im}}\boldsymbol{W}_1\boldsymbol{H}_{\mathrm{im}} + \sum_{i=1}^{k}\boldsymbol{M}'_i\boldsymbol{W}_2\boldsymbol{M}_i\Bigg] \tag{13}$$

where H_{dom} is the domain state of H, or $H(n)$, and H_{im} is the image state of H, or $H(n+1)$.

It should be noted that, in this study, we achieved a one-step (i.e., one-orbit) convergence to the target set of all of the cells in the state space of interest. Thus, as discussed in Sec. IV.B, the CSSOCT is generated directly without creating the CSST.

V. Simulation Study Results

Orbit simulations performed to validate the new unloading method are described here. The CSSOCT was generated separately for several different discrete control-level configurations and for two model spacecraft. The CSSOCT generation software and input/output structures were designed specifically for this study. The control dynamics of Eq. (11) and the cost function of Eq. (13) were employed in following the algorithm described in Sec. II.B to generate a CSSOCT in binary format. The CSSOCT was designed as a table of H_{dom} states vs M sequences. Thus, once per orbit (i.e., with a sampling period of one orbital period) the CSSOCT was accessed by the orbit simulation via a direct-access READ keyed to the current CMG angular momentum state (H_{dom}). At that time, the optimal interval control magnetic sequence M was read; this sequence was implemented for the duration of the next orbit.

Simulations of a small spacecraft and a large spacecraft with the mass properties of the NASA Gamma Ray Observatory (GRO) were performed.

A. Small Spacecraft

The small spacecraft[7] has principal moments of inertia: $I_x = 125$ kg-m^2, $I_y = 116$ kg-m^2, and $I_z = 135$ kg-m^2. The momentum exchange device is assumed to have a spherical momentum envelope of $|H|_{max} = 5$ N-m-s. The spacecraft has magnetic torquers of maximum magnetic moment $M_{max} = 50$ A-m^2. The orbit simulated is of inclination $i = 28.5$ deg and altitude 200 n.mi. An Earth-pointing desired attitude is assumed. The external disturbance torques, dominated by aerodynamic drag, are modeled by Eqs. (6). For this spacecraft, $A_y = -0.000086$ N-m, $S_y = -0.000057$ N-m, $A_z = 0.00043$ N-m, and $S_z = 0.000285$ N-m. These values are sized based on earlier studies.[8,18]

Equation (11) was applied through specifically designed software to generate the CSSOCT off-line. The state space of angular momentum H was discretized into 1000 total cells, 10 for each dimension of the three body axes. The 1000 state-space cells were assigned the values

$$H_i = \{\pm 0.5,\ \pm 1.5,\ \pm 2.5,\ \pm 3.5,\ \pm 4.5\}\ \text{N-m-s}$$

for i representing each of the three body axes x, y, and z. With this choice of discrete cell structure, we have relegated any H_i whose absolute value exceeds 5 to the sink cell. We have assumed that the entire set of 1000 cells defined is within the domain of attraction of the origin; i.e., it is a controllable set. This assumption was verified upon creation of the CSSOCT.

It is assumed that the magnetic moment control M can change every quarter-orbit [i.e., $k = 4$ in Eqs. (11) and (13)]. This control discretization is simple to implement using electromagnets, but at the same time is able to take advantage of the periodic fluctuations of the Earth's magnetic field. In this study, we restricted the control to n discrete levels, for $n = 2$, 3, 5, and 7. The control levels for each n are given in Table 1. The target set was assigned to be the innermost eight cells surrounding the origin: $H_i \in \{-0.5, 0.5\}$, $i = x,y,z$. In the generation of the CSSOCT for the $n = 2$ (two-level) control configuration, all 1000 cells converged to the target set in one mapping step (one orbit).

The significance of this, as pointed out in Sec. IV.B, is that the need to create the storage-intensive CSST was eliminated, and the CSSOCT could be generated directly. However, the CSSOCT generation CPU requirements are directly proportional to the cube (due to three components of M) of the total number of control sequences processed. As a result of resource limitations, it was impractical to process the full set of control sequences for three-, five-, and seven-level control. Instead, the three-, five-, and seven-level control sequences chosen were subsets of the full sets designed to contain the two-level sequences as a subset. This guarantees that the higher control-level configurations also converge to the target set in one step.

Table 1 Magnetic control levels

n	Small spacecraft M, A-m^2	Gamma Ray observatory M, A-m^2
2	$\{\pm 50\}$	$\{\pm 1800\}$
3	$\{0, \pm 50\}$	$\{0, \pm 1800\}$
5	$\{0, \pm 25, \pm 50\}$	$\{0, \pm 900, \pm 1800\}$
7	$\{0, \pm 12, \pm 25, \pm 50\}$	$\{0, \pm 400, \pm 900, \pm 1800\}$

The choices of which sequences to include were based subjectively on examination of the two-level (complete sequence set) CSSOCT—which two-level sequences were chosen most frequently as optimal by the algorithm.

Simulation of the attitude control system with no unloading resulted in the X and Z components of momentum remaining bounded, but the Y component possessing a linearly growing secular component. The goal of the momentum unloading control law is, therefore, to keep the Y-momentum component bounded within the ± 5 N-m-s saturation limits while maintaining the boundedness of the X and Z components. In addition, the momentum unloading torques should not significantly increase the spacecraft attitude errors.

Extensive numerical computation studies have shown that the angular momentum would stabilize within saturation bounds if a sufficient number of sequences were included in the set of possible controls. The cost function of Eq. (12) was employed with weighting matrices $W_1 = \text{diag}\ (1,1,1)$ and $W_2 = [0]$. These values of W_1 and W_2 were chosen based on good momentum unloading performance among the several tested. Thus, the optimality criterion is to minimize the angular momentum magnitude over the course of an orbit without costing the magnetic control effort. In the remainder of this section, we will discuss the results of seven-level control configurations.

1. *Seven-Level Control*

A control sequence set containing 7 levels and 46 possible sequences, denoted 7/46 control, was employed. The 46 sequences contain 16 sequences using only $\pm M_{max}$ (n = two levels); 10 sequences having $n = 3$; and 20 additional sequences serving as subsets of seven-level control. Appendix D contains a tabulation of the control sequences included in the 7/46 control set.

Figure 2 shows the performance of the 7/46 control over a 24-h period. Figure 2a demonstrates that the momentum accumulation in all axes is bounded within the ± 5 N-m-s limit. The magnitudes of the X and Z momentum unloading components are comparable to the no-unloading cases, but the Y component is also bounded in marked contrast to the no-unloading case. This is accomplished without significantly increasing the magnitude of the attitude angle errors. The control history is shown in Fig. 2b.

A variation of 7/46 control was developed in which two control sequence sets were employed, rather than the single 46-sequence set. The optimum unloading sequence is chosen from the original 46-member set if any of the momentum components is greater than w N-m-s, for $1 \le w \le 4$. The optimum sequence is chosen from an alternate set if all three momentum components are less than w N-m-s. The alternate

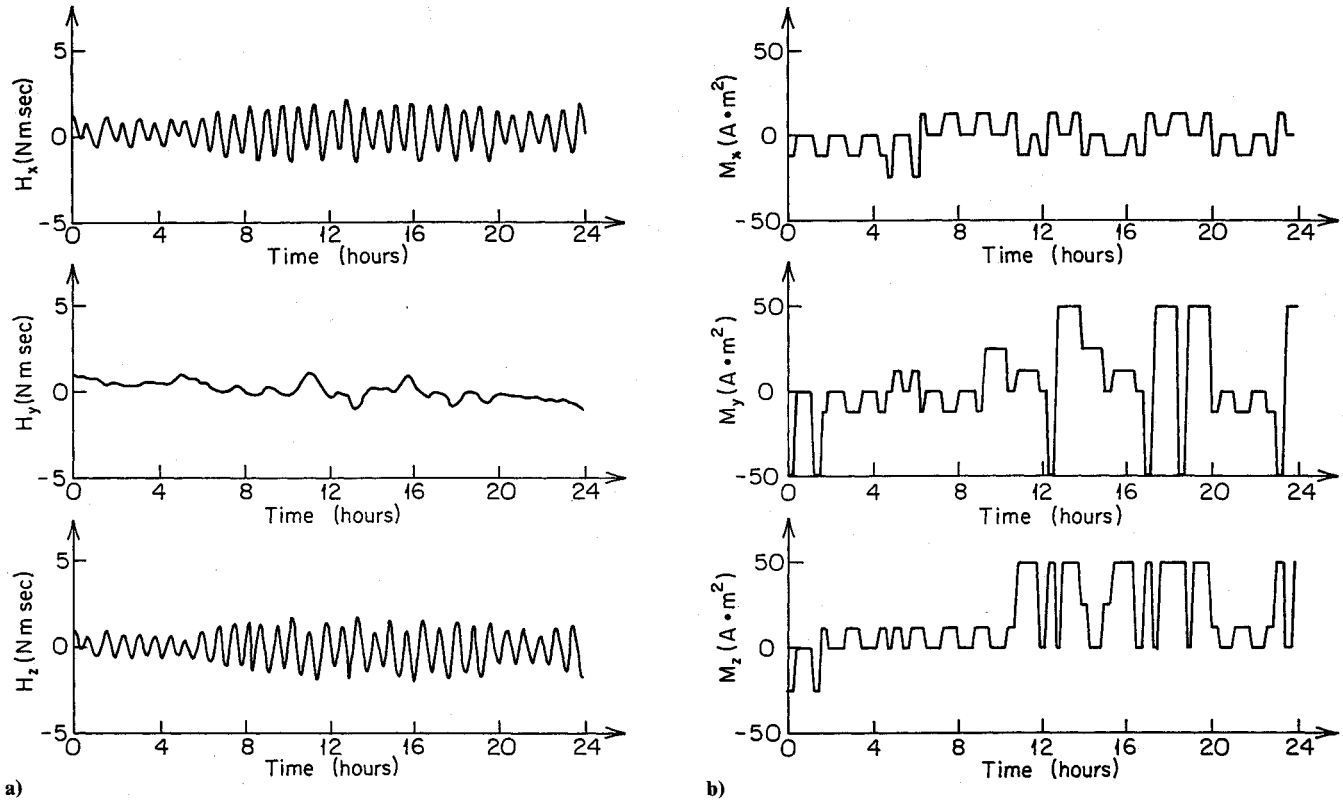

Fig. 2 7/46 control, small spacecraft: a) momentum components; b) control history.

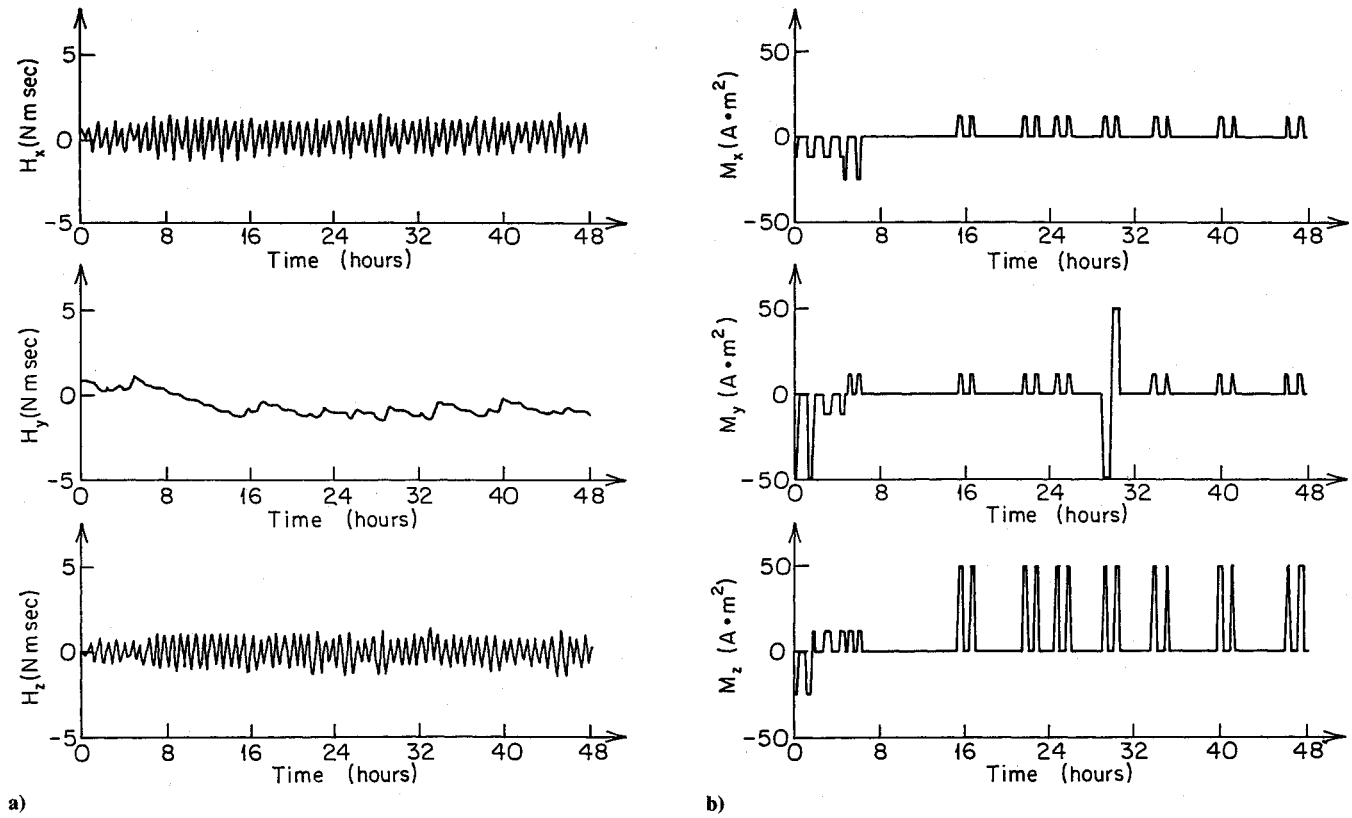

Fig. 3 Dual-sequence control, small spacecraft: a) momentum components; b) control history.

set of sequences has 45 members, all of which have no unloading for the first quarter-orbit segment. Some of the members have positive or negative unloading in the remaining orbit segments. The set containing no unloading for the entire subsequent orbit is included. The idea is to provide a magnetic sequence set of weaker controls if the momentum is relatively small. Utilizing an option to draw from more than one unloading sequence subset of a complete multilevel set of sequences in lieu of processing the complete set highlights the flexibility of the CSSOC technique.

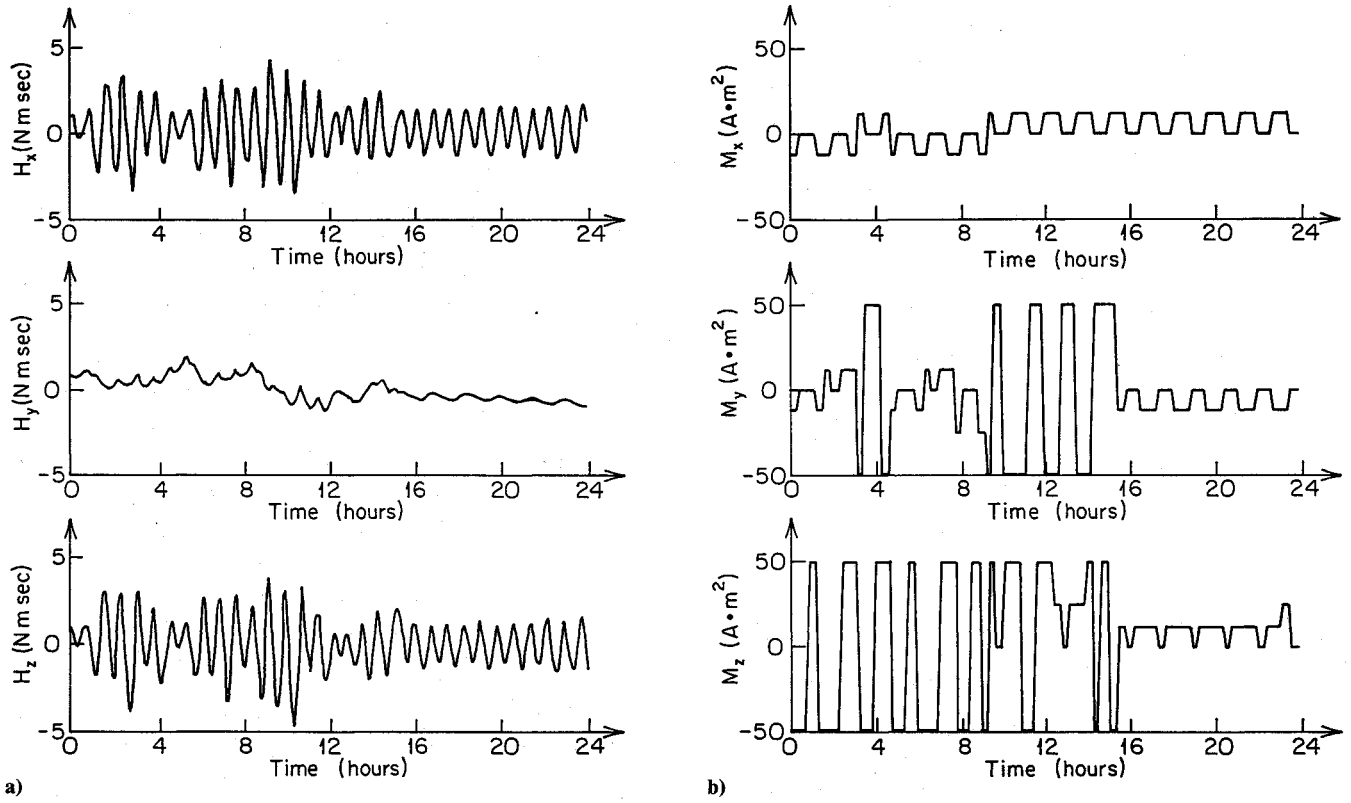

Fig. 4 Proportional cost function control, small spacecraft: a) momentum components; b) control history.

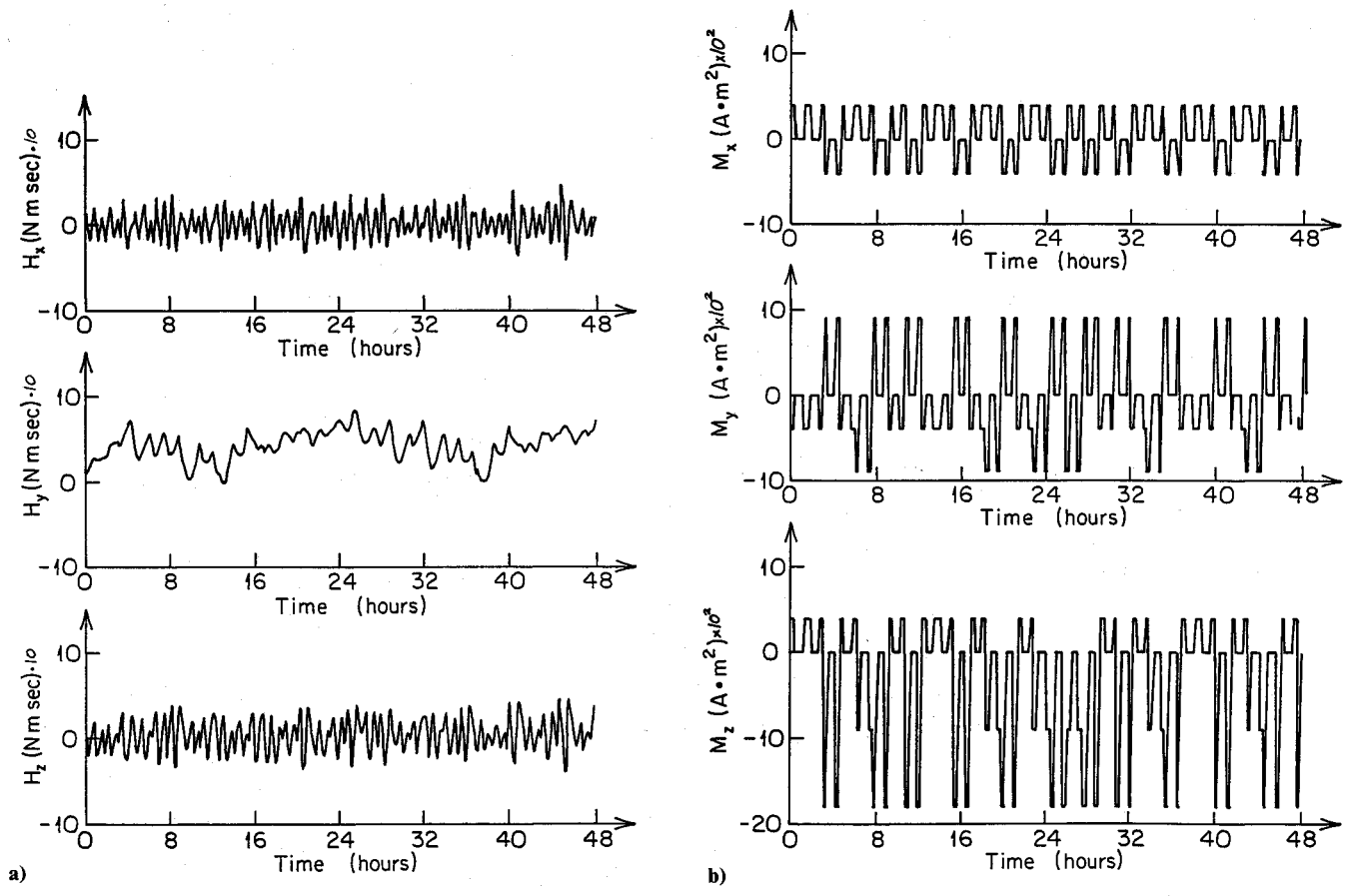

Fig. 5 7/46 control, large spacecraft: a) momentum components; b) control history.

The results of this "dual sequence set" method are shown in Fig. 3 for $w = 1$ N-m-s. We see momentum amplitudes that are even smaller than in the previous case, shown in Fig. 2a. In addition, the electromagnets performed with more off time (see Fig. 3b). Clearly, the flexibility of using dual or possibly multiple sequence sets without incurring the CPU burden of

processing a complete multilevel sequence set has shown its usefulness. Experimentation with different unloading sequences will lead potentially to additional improvements.

2. Unloading with Proportional Rather Than Integral Cost Function

This variation of the CSSOC algorithm has the optimal control sequence determined from the value of the momentum vector only at the end of an orbit. In some sense, this approach is similar to the minimum energy unloading law but, of course, the CSSOC method uses only a finite number of control levels.

In this case, rather than minimizing an integral cost function as in Eq. (12) we minimize the function

$$J = \boldsymbol{H}'\boldsymbol{H} \tag{14}$$

In implementation, the algorithm searches for a control $\boldsymbol{M}$ sequence, that drives the momentum $\boldsymbol{H}$ to the target set in one mapping step (orbit), and accepts the first such control sequence it processes as the optimal one for the domain cell of interest. The order in which the control sequences are systematically processed, therefore, has significant bearing on the eventual optimal control sequence. The designer can influence the control sequence chosen as optimal by having the algorithm process the various sequences in the chosen set according to his or her order of preference (e.g., to minimize magnetic moment).

Figure 4 shows the results of the proportional cost function variation of the CSSOC technique using the same 7/46 control sequence set as in the previous cases. Figure 4a shows that the momentum components are bounded, although with higher amplitudes than in the previous cases (see Figs. 2 and 3). This is despite the fact that the information about the momentum includes only its magnitude at one point in the orbit. As anticipated, simplifying the analysis process results in lower performance. The performance in this proportional cost-function variation can be improved by increasing the number of control levels and the number of possible control sequences.

B. Large Spacecraft

The large spacecraft modeled possesses the physical characteristics of the NASA Gamma Ray Observatory. The orbit/attitude features were assumed to be the same as with the small spacecraft. The large spacecraft model possesses the following parameters: $I_x = 50{,}760$ kg-m^2, $I_y = 79{,}550$ kg-m^2, $I_z = 95{,}260$ kg-m^2, and $H_i = \{\pm 20, \pm 60, \pm 100, \pm 140, \pm 180\}$ N-m-s. The maximum magnetic moment $M_{\max}$ is 1800 A-m^2. The external disturbance model, although still of the form of Eqs. (6), has the following coefficient values: $A_y = 0.0085$ N-m, $S_y = 0.00275$ N-m, $A_z = 0.00425$ N-m, and $S_z = 0.0014$ N-m.

The large spacecraft with no unloading experiences the Y component of momentum growing unbounded, as in the case of the small spacecraft. Employing the same cost function and weighting matrices as for the small spacecraft, we again simulated 7/46 control. The 46 sequences of magnetic moments possess a one-to-one correspondence with those listed in Appendix D and have the seven levels shown in Table 1. Figure 5 shows the momentum and control histories, respectively, for the big spacecraft under 7/46 control. It is seen that the CSSOC method also is successful at achieving tightly bounded momentum for the large spacecraft.

VI. Conclusions

This paper has presented the application of the cell mapping technique developed by C. S. Hsu to the spacecraft momentum unloading problem. We have demonstrated through orbit simulation how a near-instantaneous table-read once per orbit enabled two spacecraft of widely differing characteristics to maintain momentum control. We have presented a variety of optimal control inputs generated by the new cell state space optimal control technique, which succeeded in controlling momentum buildup. The approach presented could provide a spacecraft near-autonomous momentum control if the optimal control table of values was stored in the onboard computer. Since cell mapping discretization allows analysis of nonlinear and time-varying problems, it has many potential applications in development of spacecraft momentum unloading algorithms and also can be applied to other spacecraft control problems. Future studies may focus on developing more efficient and rapid search techniques to generate optimal control sequences.

Appendix A: Coordinate Systems

Reference coordinate frame:

X axis pointing in direction of travel

Y axis perpendicular to orbit plane to form a right-handed set

Z axis pointing toward nadir

Body Coordinate frame:

X, Y, Z axes fixed to body to be coincident to reference frame in nominal Earth-pointing unperturbed flight; aligned with spacecraft principal axes.

Appendix B: Attitude Dynamics and Control Equations for Momentum Unloading Algorithm Validation

The attitude dynamics are derived by assuming small attitude angles and low angle rates. The body rates are expressed in terms of the Euler angle rates in an Earth-pointing configuration for the rotation sequence: roll, ϕ, about the X axis; pitch, θ, about the Y axis; yaw, ψ, about the Z axis. Spacecraft dynamics follow from the Euler equations:

Roll:

$$\ddot{\phi} = [4\omega_0^2(I_z - I_y)\phi + \omega_0(I_z - I_y + I_x)\dot{\psi} + \omega_0 h_{cz} + T_{cx} + T_{dx} + \omega_0 h_{cy}\phi + h_{cy}\dot{\psi}]/I_x$$

Pitch:

$$\ddot{\theta} = [3\omega_0^2(I_z - I_x)\theta + T_{cy} + T_{dy}]/I_y$$

Yaw:

$$\ddot{\psi} = [\omega_0^2(I_x - I_y)\psi + \omega_0(I_y - I_x - I_z)\dot{\phi} - \omega_0 h_{cx} + T_{cz} + T_{dz} + \omega_0 h_{cy}\psi - h_{cy}\dot{\phi}]/I_z$$

Roll momentum:

$$\dot{h}_{cx} = -T_{cx}$$

Pitch momentum:

$$\dot{h}_{cy} = -T_{cy}$$

Yaw momentum:

$$\dot{h}_{cz} = -T_{cz}$$

The following proportional/rate attitude control law is employed:

Roll:

$$T_{cx} = -K_{rx}\dot{\phi} - K_{py}\phi - 4\omega_0^2(I_z - I_y)\phi - \omega_0(I_z - I_y + I_x)\dot{\psi} - \omega_0 h_{cz} - \omega_0 h_{cy}\phi - h_{cy}\dot{\psi}$$

Pitch:

$$T_{cy} = -K_{ry}\dot{\theta} - K_{py}\theta - 3\omega_0^2(I_z - I_x)\theta$$

Yaw:

$$T_{cz} = -K_{rz}\dot{\psi} - K_{pz}\psi - \omega_0^2(I_x - I_y)\psi - \omega_0(I_y - I_x - I_z)\dot{\phi} + \omega_0 h_{cx} - \omega_0 h_{cy}\psi + h_{cy}\dot{\phi}$$

The attitude control law generates control torques proportional to attitude angles and attitude rates. The controller also incorporates uncoupling terms, which negate all cross-axis effects except momentum unloading and aerodynamic torques, similar to the controllers of Shain and Spector[2] and Junkins et al.[7]

Appendix C: Earth Magnetic Field Models

The components of the tilted dipole model of the magnetic field in reference coordinates are as follows:

$$B_{rx} = A\cos\alpha + (-B + C)\cos\alpha\cos\mu - (B + C)\sin\alpha\sin\mu \quad \text{(C1a)}$$

$$B_{ry} = -D - E\cos\mu \quad \text{(C1b)}$$

$$B_{rz} = 2A\sin\alpha - (2B - 2C)\sin\alpha\cos\mu + (2B + 2C)\cos\alpha\sin\mu \quad \text{(C1c)}$$

where

$$A = (\mu_e/r^3)\cos\epsilon\sin i$$

$$B = (\mu_e/2r^3)\sin\epsilon(1 + \cos i)$$

$$C = (\mu_e/2r^3)\sin\epsilon(1 - \cos i)$$

$$D = (\mu_e/r^3)\cos\epsilon\cos i$$

$$E = (\mu_e/r^3)\sin\epsilon\sin i$$

and

M_e = Earth dipole moment

ϵ = dipole tilt angle

Δ = magnetic dipole east longitude

$\mu = \lambda_G + \Delta - \Omega$

λ_G = angle from vernal equinox east to Greenwich meridian

Ω = orbit right ascension

α = true anomaly + argument of perigee

i = orbit inclination

r = distance from Earth center to spacecraft

For a derivation of these equations, see Ref. 15.

Equations (C1) are easily reduced to a straight dipole model by letting $\epsilon = 0$. Then we have the following:

$$B_{rx} = A\cos\alpha \quad \text{(C2a)}$$

$$B_{ry} = -D \quad \text{(C2b)}$$

$$B_{rz} = 2A\sin\alpha \quad \text{(C2c)}$$

Note that Eqs. (C2) are periodic with the orbital period.

Appendix D: Available Control Sequences for 7/46 Control

The following set of 46 control sequences is used in 7/46 control. Each group of four numbers represents four sequential quarter-orbit interval hold values of any of the three components of magnetic torquer dipole moment M. Thus, each four-member group offers a control option for a full orbit. The last section of 16 groups represents the complete two-level control sequence set, which serves here as a subset of seven-level control. The other groupings of 10 represent other subsets of seven-level control. The units are amperes per square meter.

(12,0,0,12)	(−12,0,0,−12)	
(0,12,0,12)	(0,−12,0,−12)	
(−12,0,−12,0)	(12,0,12,0)	
(−12,−12,0,−12)	(12,0,12,12,)	
(12,12,12,0)	(−12,0,−12,−12)	
(25,0,0,25)	(−25,0,0,−25)	
(0,25,0,25)	(0,−25,0,−25)	
(−25,0,−25,0)	(25,0,25,0)	
(−25,−25,0,−25)	(25,0,25,25)	
(25,25,25,0)	(−25,0,−25,−25)	
(50,0,0,50)	(−50,0,0,−50)	
(0,50,0,50)	(0,−50,0,−50)	
(−50,0,−50,0)	(50,0,50,0)	
(−50,−50,0,−50)	(50,0,50,50)	
(50,50,50,0)	(−50,0,−50,−50)	
(−50,50,−50,50)	(50,−50,50,−50)	
(−50,50,−50,−50)	(50,−50,50,50)	
(−50,50,50,−50)	(50,−50,−50,50)	Original
(−50,−50,50,−50)	(50,50,−50,50)	two-level
(50,−50,−50,−50)	(−50,50,50,50)	control
(50,50,50,−50)	(−50,−50,−50,50)	sequence
(−50,−50,50,50)	(50,50,−50,−50)	set
(−50,−50,−50,−50)	(50,50,50,50)	

References

[1]Woo, H. H., Morgan, H. D., and Falangas, E. T., "Momentum Management Concepts for a Space Station," AIAA Paper 86-2047, Aug. 1986; also, Woo, H. H., Morgan, H. D., and Falangas, E. T., "Momentum Management and Attitude Control Design for a Space Station," *Journal of Guidance, Control, and Dynamics,* Vol. 11, Jan. 1988, pp. 19-25.

[2]Shain, E. B. and Spector, V. A., "Adaptive Torque Equilibrium Control of the Space Station," AIAA Paper 85-0028, Jan. 1985.

[3]Schmidt, G. E. and Muhlfelder, L., "The Application of Magnetic Torquing to Spacecraft Attitude Control," American Astronautical Society Paper 81-002, Feb. 1981.

[4]Mobley, F. F., Tossman, B. E., Fountain, G. H., and Heffernan, K. J., "Use of Magnetics in Attitude Control at APL," American Astronautical Society Paper 81-001, Feb. 1981.

[5]Goetz, R. E., "The Use of Magnetic Torquing for Control Moment Gyro Desaturation," NASA Project TR NAS 9-8166, Dec. 1969.

[6]Levidow, W., "Use of Magnetic Torque for CMG Momentum Management," BellCom, Inc., Washington, DC, TM-69-1022-8, Dec. 1969.

[7]Junkins, J. L., Rajaram, S., Baracat, W. A., and Carrington, C. K., "Precision Autonomous Satellite Attitude Control Using Momentum Transfer and Magnetic Torquing," *The Journal of the Astronautical Sciences,* Vol. 30, Jan. 1982.

[8]Decanini, J. H., Flashner, H., and Schmeichel, H., "Magnetic Control and the 25 KW Power System," American Astronautical Society Paper 81-004, Feb. 1981.

[9]Hsu, C. S., "A Theory of Cell-to-Cell Mapping Dynamical Sys-

tems," *Journal of Applied Mechanics,* Vol. 47, Dec. 1980, pp. 931–939.

[10]Hsu, C. S. and Guttalu, R. S., "An Unravelling Algorithm for Global Analysis of Dynamical Systems: An Application of Cell-to-Cell Mappings," *Journal of Applied Mechanics,* Vol. 47, Dec. 1980, pp. 940–948.

[11]Guttalu, R. S., "On Point Mapping Methods for Studying Nonlinear Dynamical Systems," Ph.D. Dissertation, Dept. of Mechanical Engineering, Univ. of California, Berkeley, CA, March 1981.

[12]Hsu, C. S., "A Generalized Theory of Cell-to-Cell Mapping for Nonlinear Dynamical Systems," *Journal of Applied Mechanics,* Vol. 48, Sept. 1981, pp. 634–642.

[13]Hsu, C. S., *Cell-to-Cell Mapping,* Springer-Verlag, New York, 1987.

[14]Hsu, C. S., "A Discrete Method of Optimal Control Based Upon the Cell State Space Concept," *Journal of Optimization Theory and Applications,* Vol. 46, Aug. 1985, pp. 547–569.

[15]Wheeler, P. C., "Magnetic Attitude Control of Symmetric Spinning Satellites," Ph.D. Dissertation, Dept. of Aeronautics and Astronautics, Stanford Univ., Stanford, CA, April 1965.

[16]Alfriend, K. T. and Lindberg, R. E., "Geomagnetic Field Effects on the Design of a Magnetic Attitude Control System," *Journal of the Astronautical Sciences,* Vol. 27, July 1979, pp. 269–292.

[17]Eller, T. J. and Wagie, D. A., "Earth's Magnetic Field Models for Dumping Momentum Magnetically on GPS Satellites," *Journal of Guidance and Control,* Vol. 5, Sept.–Oct. 1982, pp. 438–441.

[18]Hughes, P. C., *Spacecraft Attitude Dynamics,* Wiley, New York, 1986, pp. 232–273.